



Effect of warm forming process parameters on 42CrMo4 skew rolled bar mechanical properties and microstructure

Alberto Murillo-Marrodán¹ · Tomasz Bulzak² · Eduardo García¹ · Hamed Aghajani Derazkola¹ · Krzysztof Majerski² · Janusz Tomczak² · Zbigniew Pater²

Received: 11 July 2023 / Revised: 11 January 2024 / Accepted: 12 February 2024
© The Author(s) 2024

Abstract

Skew rolling is a manufacturing process in which two or three rolls are used to reduce the diameter or modify the shape of a cylindrical workpiece, which is used to manufacture mechanical components such as shafts, rods or balls. Hot conditions are used to overcome limitations related to material ductility, residual stress and machine capacity. In this paper, the warm skew rolling (WSR) process of 42CrMo4 rods is modeled by the finite element method. The effects of forming parameters, namely initial temperature and roll rotational velocity, on the material strain rate, thermal properties, microstructure and hardness were analyzed. Simulation results were validated by experimental process data, while hardness tests and SEM-EBSD microscopy were used to assess mechanical properties and microstructure, respectively. The WSR resulting microstructure is different from the normalized ferritic–pearlitic initial one. The degree of spheroidization (DoS) of cementite increases with temperature. The maximum DoS of 86.5% occurs at the initial temperature of 750 °C, leading to the highest material softening. Rolling from lower temperatures favors grain fragmentation and the achievement of incomplete spheroidization, which, in combination with the highest proportion of high-angle boundaries, contributes to a higher hardness of the rods with respect to those rolled at higher temperatures. The highest reduction in hardness takes place at 750 °C and 30 rpm, leading to 209.4 HV1 (30.7% reduction) and 194.1 HV1 (35.7% reduction) in the near-surface and internal regions, respectively. The driving factor is the transformation of cementite precipitates into a spheroidal form characterized by the greatest degree of dispersion.

Keywords Skew rolling · Warm forming · Mechanical properties · Microstructure · Spheroidization

1 Introduction

Skew rolling technologies are widely employed in the manufacturing process of mechanical components such as shafts, tubes, cylindrical bars and balls [1]. This process is carried out by means of two or three rollers (barrel-shaped or conical) arranged obliquely to the axis of the bar to be manufactured. In the case of round bar manufacturing methods, the process is generally conducted in hot instead of cold conditions to overcome limitations related to material ductility,

residual stress and machine capacity [2]. In fact, one of the major limitations is the development of ductile fractures in the axis of rolled products, although the use of high feed angles has been shown to help eliminate this problem [3]. Nevertheless, there are alternatives such as warm forming, which reduces some of the aforementioned limitations and presents advantages compared to hot formed ones, namely better tolerances achieved, the reduced roughness of the surfaces, there is no scale, and decarburization is reduced [4]. In addition, there is a reduction in the overall process energy consumption [5]. However, there are some drawbacks. The force required is the major one. Huang et al. [6] stated that forces were up to three times higher in a warm skew rolling (WSR) process compared to the equivalent process in hot conditions.

Among the materials commonly used to manufacture cylindrical bar and tubular products by rolling methods, the 41XX high-strength low-alloy family is very prominent due

✉ Alberto Murillo-Marrodán
alberto.murillo@deusto.es

¹ Department of Mechanics, Design and Industrial Management, University of Deusto, Avda Universidades 24, 48007 Bilbao, Spain

² Lublin University of Technology, Nadbystrzycka 36, 20-618 Lublin, Poland

Table 1 Chemical composition of 42CrMo4 steel

C	Cr	Mn	Si	P	S	Ni	Mo	Fe
0.42	0.96	0.89	0.18	0.006	0.007	0.12	0.17	Rest

to its good mechanical properties, toughness and fatigue strength [7]. These steels are commonly formed at high temperatures, ranging between 900 and 1250 °C [8], followed by quenching in oil [9] or water–air [10] systems and, after that, a subsequent tempering heat treatment to get the

final desired properties. When machining or cold-forming is required, annealing heating processes are performed [11]. It is therefore a long and energy-intensive process and, as mentioned above, efforts are being made to investigate the warm fabrication of structures with very different objectives,

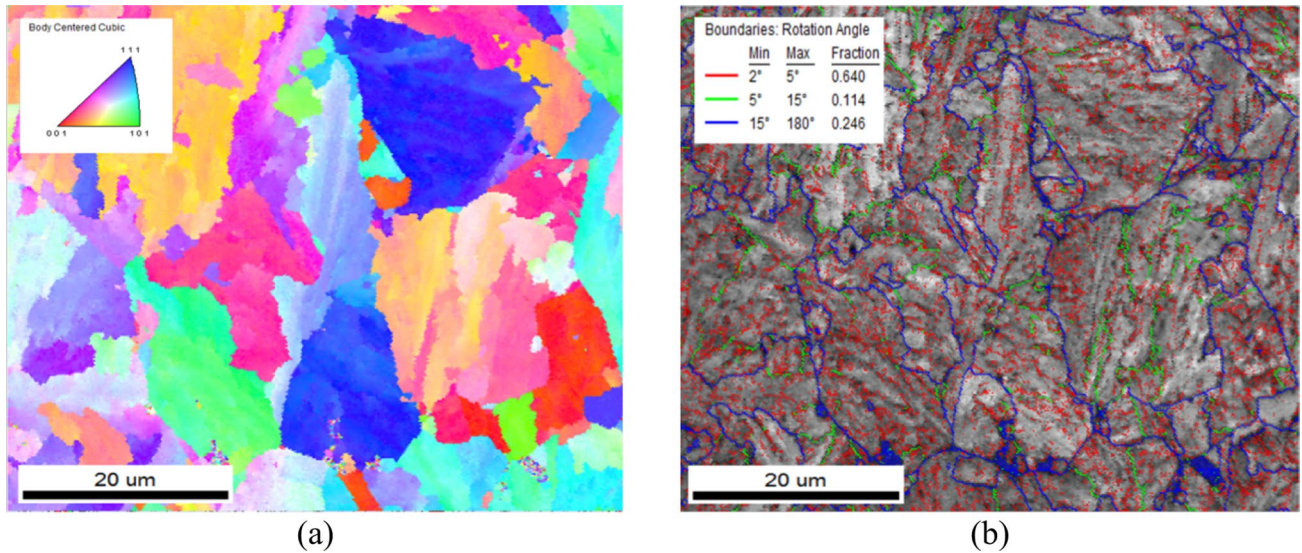


Fig. 1 Results of the EBSD analysis of initial microstructure: (a) misorientation profile map and (b) grain boundary misorientation

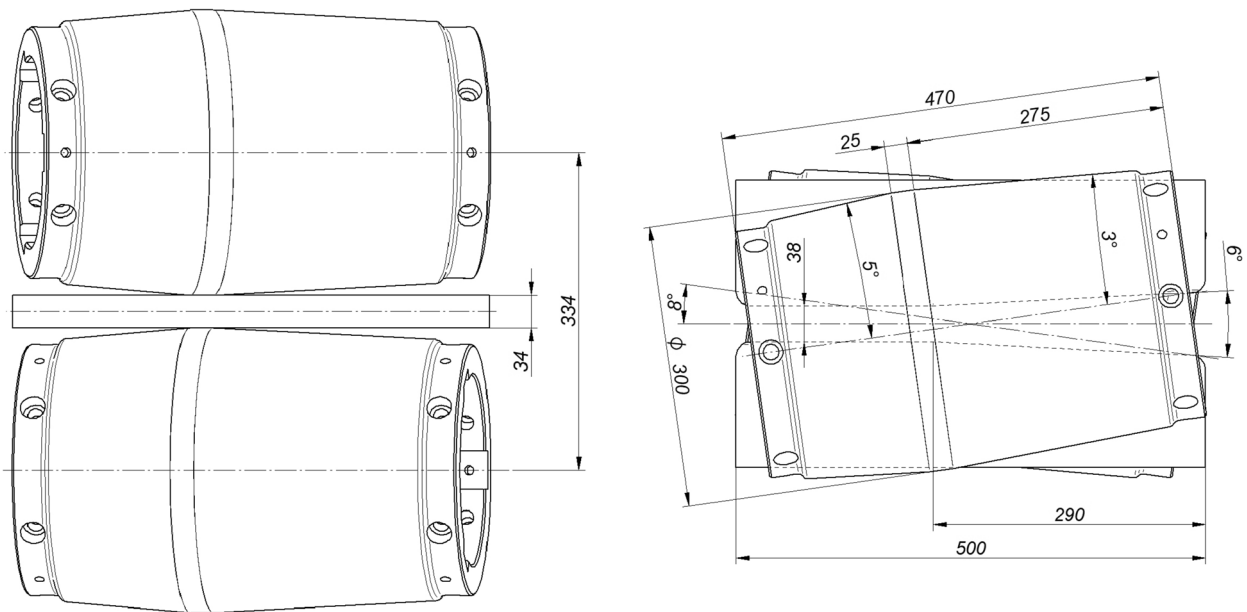
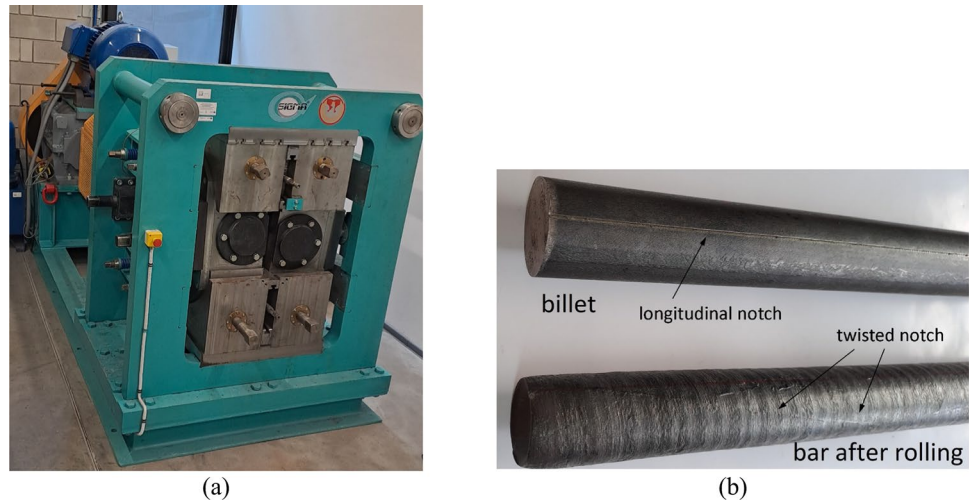


Fig. 2 Schematic view and geometrical dimensions of rolls and guiding elements

Fig. 3 The skew rolling stand (a) view from the input side and (b) bar twisting experimental measures



on the one hand refined-grain structures that compete with hot-processed, quenched and tempered ones [12], and soft structures that can be machined and cold-formed without prior annealing [13]. Within the WSR of 41XX steels, the most researched variants are warm cross wedge rolling (WCWR), warm forging (WF) and warm skew rolling of steel balls (WSRB).

In the WCWR of 42CrMo steel, a dispersing spheroidized cementite on ferrite matrix was found, which resulted in lower hardness and tensile strength, but higher elongation and machinability [6]. Shu et al. [14] investigated the effect of WCWR parameters on the surface quality of 42CrMo shafts. The reduction ratio was directly linked to worse surface quality of the workpiece, and the optimum working temperature for this material was in the range of 700–800°C. The WCWR has also been analyzed for high carbon steel rods, the desired output of the WCWR was the development of a microduplex ferrite–cementite structure, starting from pearlite [15]. In the outer region, fully spheroidized cementite particles were found, while in the interior, partial fragmented lamellar cementite was observed [13]. In addition, dynamic continuous recrystallization of ferrite was observed in the whole cross-section but with different degrees depending on the location, which generated differences in the mechanical properties (yield strength and plasticity).

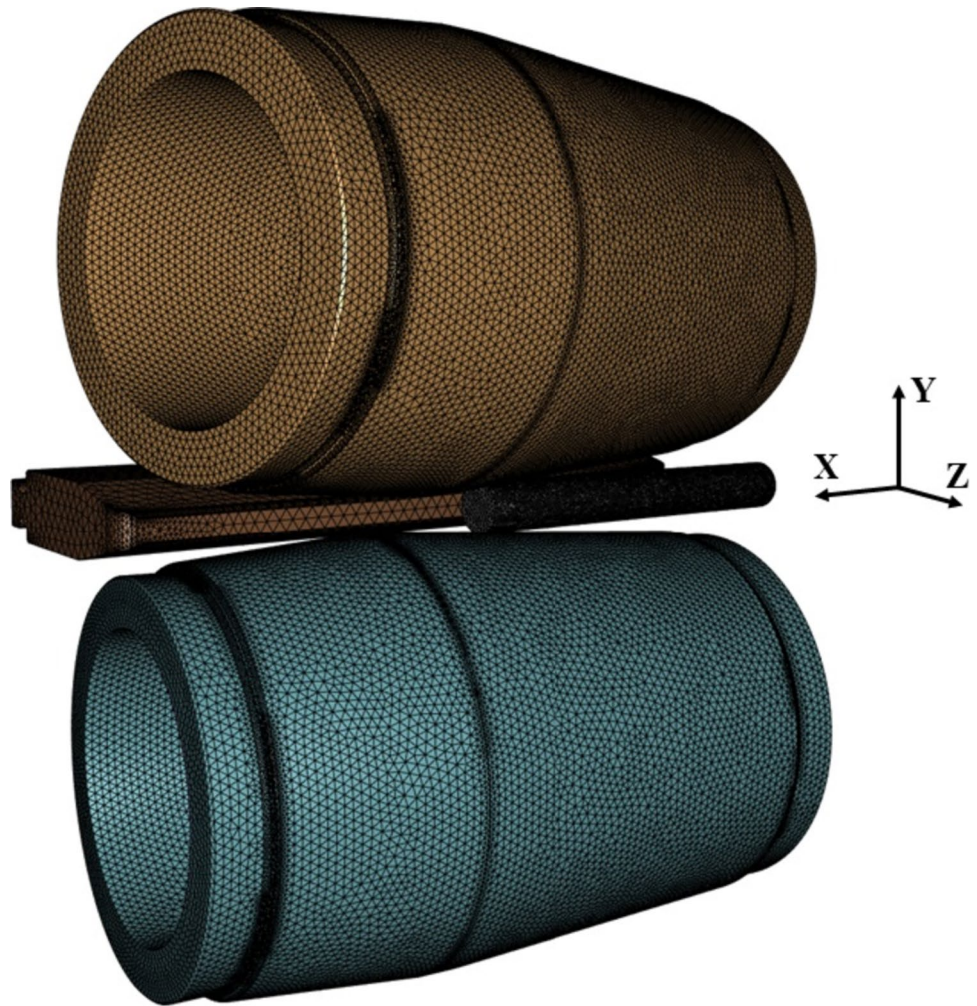
The WF of bevel gear of 42CrMo4 steel was investigated by Lee et al. [16]. The forming temperature was set between A3 and A1, which lead to a final refined ferrite–pearlite grain structure, with a more homogeneous microstructure compared to conventional hot forging. Cui et al. [17] analyzed the same material in a variation of the WSR of spline shafts. The optimum forming temperature was determined (700 °C) as a compromise between tool precision and

process efficiency. Concerning low carbon steels, Serajzadeh [18] investigated the dynamic strain aging under 360°C and at low rolling speeds, leading to serrated flow stress. The kinetics of static strain aging could be mainly affected by the rolling speed [19]. In a posterior research, it was also highlighted the importance of temperature, rolling speed and area reduction on the microstructure developed in low carbon warm-rolled steels [20]. The variation in the rolling speed modified the yield strength of the material, as it altered the dislocation pattern and subsequent nucleation rate during early stages of recrystallization.

Regarding WSRB, Huo et al. [21] investigated possibility of producing spherical components by finite element analysis (FEA) of the process. In a posterior research [22], a novel material model for 52100 bearing steel allowed identifying the carbide phase volume fraction and its spheroidization. In some regions, rectangular carbides were found due to incomplete carbide spheroidization. Under some deformation conditions, carbide agglomeration was detected.

From the literature reviewed, one of the most challenging issues in warm forming is the correct understanding of the relationship between forming conditions and the final material microstructure and properties. An important aspect that has not been investigated in depth is the impact of contact conditions in warm forming, as they alter the strain, strain rate and temperature distributions in the cylindrical bar section. In this article, experiments and simulations are used to evaluate the impact of friction and forming parameters, namely temperature and rolling speed, on the 42CrMo4 warm skew rolled rod with the aim of achieving a final microstructure ready to be machined or cold-formed without prior annealing.

Fig. 4 Mesh used in the FEM model of WSR (left shoe is not represented)



2 Materials and methods of research

2.1 Rod material

In this study, the rod has been manufactured from a 42CrMo4 steel bar provided from local market. The composition is presented in Table 1.

The initial microstructure of the bar was analyzed using scanning electron microscopy (SEM) and electron backscatter diffraction (EBSD). In order to characterize different regions, the microstructure of external, mid-radius and central area of the bar transverse section was analyzed. The EBSD analysis of the initial material as-received is presented in Fig. 1. The initial material state presents a homogeneous microstructure without different kinds of inclusions. The microstructure of 42CrMo4 steel in the normalized state has a ferritic–pearlitic structure and consists of regular grains, in the interior of which finely lamellar pearlite and ferritic areas occur. The hardness of the bar in both the internal and external area was ~ 307.1 HV1 and ~ 301.8 HV1, respectively.

2.2 Warm skew rolling process

The WSR process was performed experimentally in a two-roll set skew rolling mill in Lublin University of Technology, using barrel-shaped rolls and shoes as guiding elements. The schematic view of the process and associated geometrical dimensions used in this research are given in Fig. 2.

The skew rolling mill counts with two working rolls and two guiding shoes (see Fig. 3a). The rolls present a biconical gauge with entry angle $\varphi_1 = 5^\circ$ and exit angle $\varphi_2 = 3^\circ$, respectively. The feed angle of the rolls was set to $\beta = 8^\circ$. The separation of the rolls at the gorge (region of minimum separation between them) was 34 mm. The material of the rolls was 55NiCrMoV6 with roll surface hardness of 40 HRC and roughness $R_a = 1.7 \mu\text{m}$. Two different rotational speeds were used for the working rolls, namely 15 and 30 rpm. Guide shoes were made of 55NiCrMoV6 with hardness of 40 HRC. A rolled round bar with the diameter of 36 mm and length of 300 mm was used as the initial bar. The heating process of the bar took place on a chamber-type electric resistance furnace up to the working temperatures of 650 and 750 °C

Table 2 List of the cases simulated and the conditions used

Case N°	Initial temperature, T (°C)	Rotation velocity, N (rpm)	Friction coefficient m (–)
1	650	15	0.55
2	650	15	0.6
3	650	15	0.65
4	650	30	0.55
5	650	30	0.6
6	650	30	0.65
7	750	15	0.55
8	750	15	0.6
9	750	15	0.65
10	750	30	0.55
11	750	30	0.6
12	750	30	0.65

for 15 min. The transportation time of the billets from the furnace to the inlet of the skew rolling mill was ~ 15 s.

The dimensions of the bar after skew rolling, the torque exerted by the working rolls, the velocity of the bar at the exit of the rolling mill, and the material surface twisting were recorded during the experiment. The average diameter was measured at four different points along the length of the bar. The cable displacement transducer WObit was used for recording the velocity of the bar during the rolling operation. The twisting of the material along the length of the bar was measured by generating a longitudinal notch in the bar, which was measured after rolling (Fig. 3b). Then, bars were cooled down to ambient temperature under natural air conditions. For further research, sections were cut out from the area 100 mm apart from the bar head end, where the process has reached steady temperature and deformation conditions.

From the bar sections, hardness measurements were taken at different positions of the bar radius using the FM800 Futuretech equipment, covering from the outer region to the central axis. In addition, SEM images were taken from these regions, in some of the tested conditions, to analyze the effect of working rolls rotational velocity (N) and initial temperature (T) on the microstructure. Microstructure studies were carried out on metallographic scrap produced on cross sections of the warm-rolled bars. The specimens were cut using an abrasive cutting machine with water cooling. The specimens were grinded on abrasive papers with grits of 80, 220, 320, 600, and 1200, respectively, and then the specimens were polished using 3 μm diamond suspension and 0.05 μm colloidal silica suspension. Nital 4% was used to etch the microstructure. The near-surface region, located at mid-radius, and the central region of the warm-rolled bars were analyzed. Furthermore, in the near-surface region, EBSD was used to study crystallographic orientation and grain boundaries.

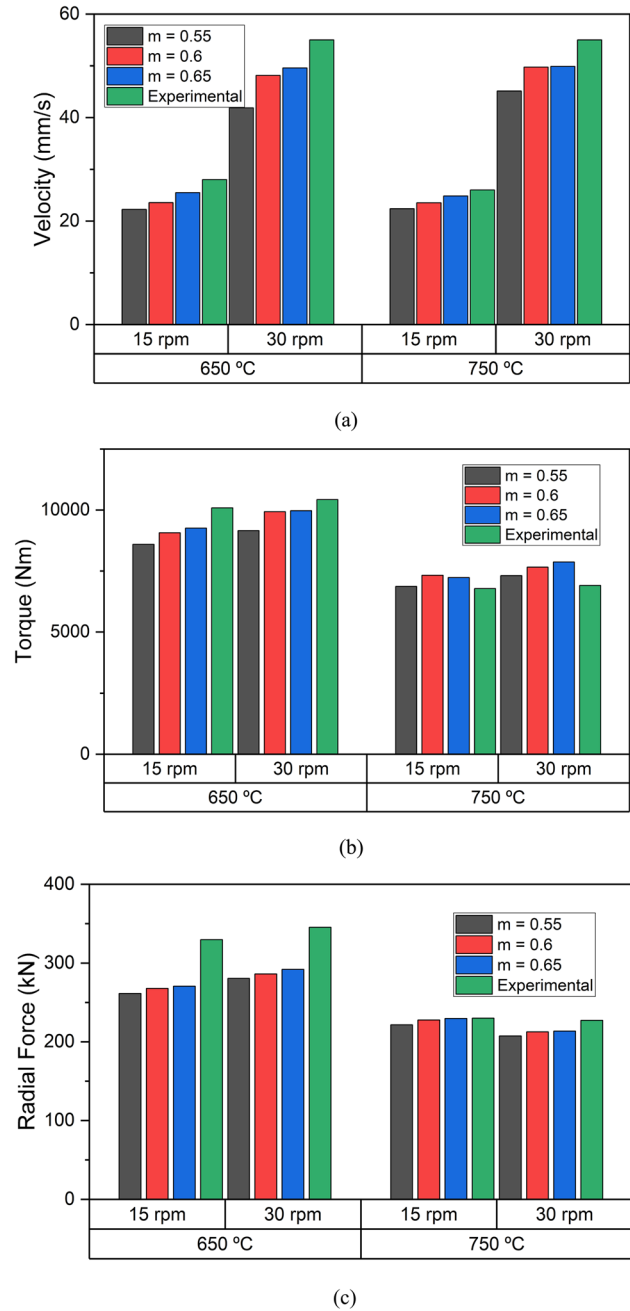
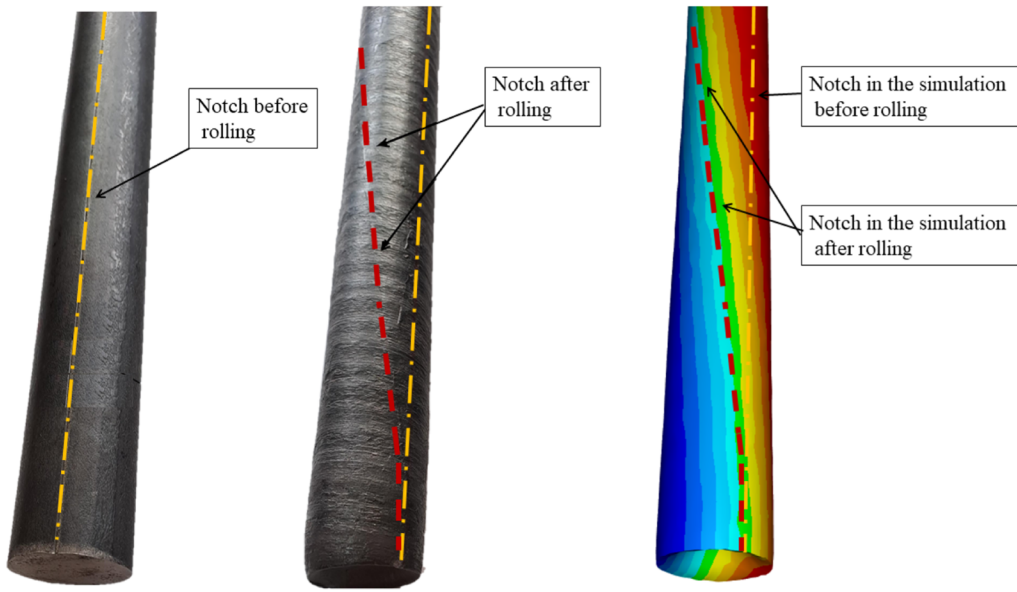


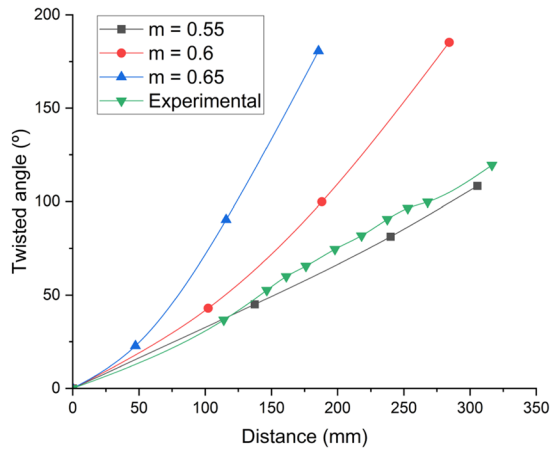
Fig. 5 Results of (a) rod velocity in the rolling direction, (b) torque exerted by the rolls and (c) radial force in the rolling mill

2.3 Process modeling and simulation

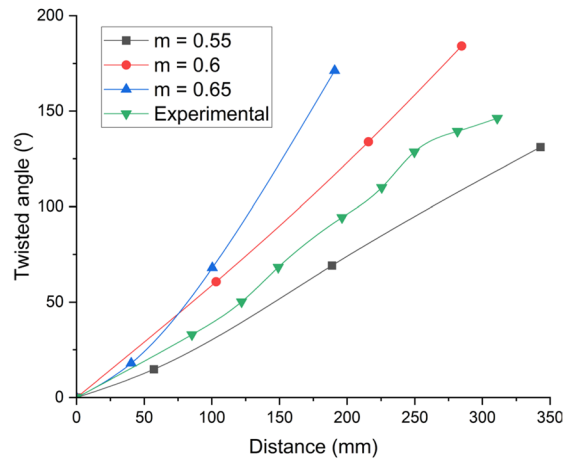
The WSR process was modeled and simulated by finite element method (FEM). The FEM model of the skew rolling mill was developed in FORGE NxT. The flow stress of the 42CrMo4 steel is dependent on the working conditions, namely temperature, strain rate and strain according to:



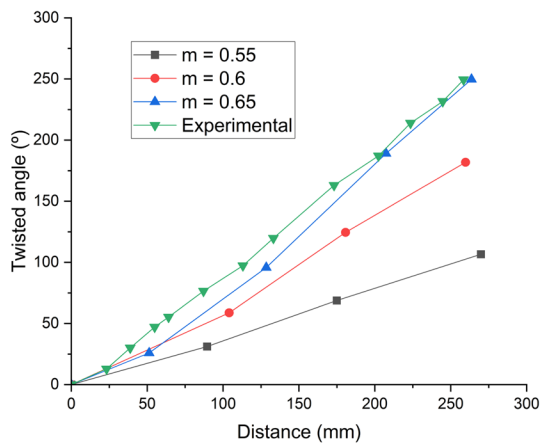
(a)



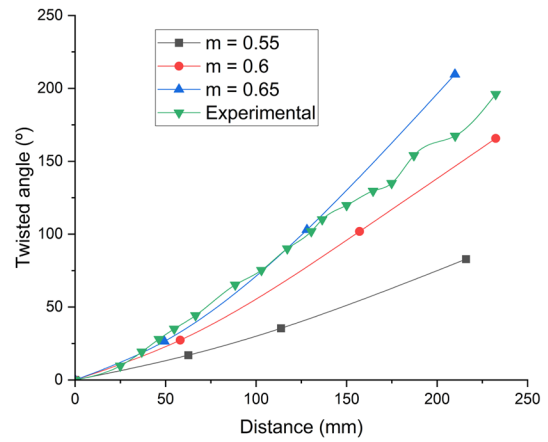
(b)



(c)



(d)



(e)

Fig. 6 Results of longitudinal surface twisting (a) experiment and simulation measurement, (b) 650 °C and 15 rpm, (c) 650 °C and 30 rpm, (d) 750 °C and 15 rpm and (e) 750 °C and 30 rpm

$$\sigma = 1872.07 \cdot e^{-0.0029T} \cdot \varepsilon^{-0.1123} \cdot \dot{\varepsilon}^{0.1437} \cdot e^{-0.0488/\varepsilon} \quad (1)$$

where σ is the flow stress, T is the temperature, ε is the strain and $\dot{\varepsilon}$ is the strain rate. The billet was considered to be elastic-viscoplastic according to Eq. 1, while working rolls and guiding shoes were defined as rigid. Those elements modeled as rigid used 2D triangular elements, while 3D tetrahedral P1 + linear elements with bubble node were assigned to the deformable ones. The element size was 6 mm for the rolls, 10 mm for the shoes and 3 mm for the billet. The resulting mesh is shown in Fig. 4.

The thermal expansion of the billet was considered during heating and WSR by updating the initial geometry of the billet according to a linear expansion coefficient of $1 \cdot 10^{-5} \text{ }^\circ\text{C}$ [23]. Furthermore, the initial billet temperature before WSR was defined considering the cooling of the bar during the transport period between the furnace and the skew rolling mill (using natural convection with air). The two initial temperatures considered in this study were 650 and 750 °C, which correspond to the in-furnace temperature. The ambient temperature was set to 20 °C, and the temperature of the dies was set to 250 °C for the working rolls and 20 °C for the guiding shoes. There was not any initial load in terms of stress or strain on the billet. The heat transfer through radiation, convection and contact between solids were taken into consideration. Regarding friction conditions, two different friction models were considered initially for modeling the skew-roll and billet contact, namely viscoplastic and shear friction models. The election of these two models is due to the fact that both showed the best performance under hot rolling conditions [24]. After several simulation tests and comparisons with experimental results, the viscoplastic friction model was not considered because at a similar billet velocity to the experimental one, the torque of the rolls was underestimated, and the material twisting overestimated. Thus, the shear friction model was used for the simulation of friction between the billet and other components under warm forming conditions [17]. The shear stress was determined by

$$\tau = m \cdot K \quad (2)$$

where m is the friction factor and K is the material consistency, which is determined by

$$K = \frac{\sigma_{eq}}{\sqrt{3}} \quad (3)$$

The contact conditions between rollers and billet vary according to the temperature and relative velocity. In order to test the effect of contact conditions on material flow and

mechanical properties and to identify which friction coefficient reproduces the different test conditions, it was initially set to $m=0.55$, $m=0.6$ and $m=0.65$. The friction with the guiding shoes was set to $m=0.3$ and kept constant during this study. Regarding the heat transfer coefficients used for the simulation, free convection with ambient media was assumed, emissivity was set to 0.5, and the contact conductance HTC was 10.000 W/m²K. In summary, two rotational speeds of the working rolls, two different initial temperatures and three friction coefficients per condition have been simulated. The simulated cases are listed in Table 2.

3 Results and discussion

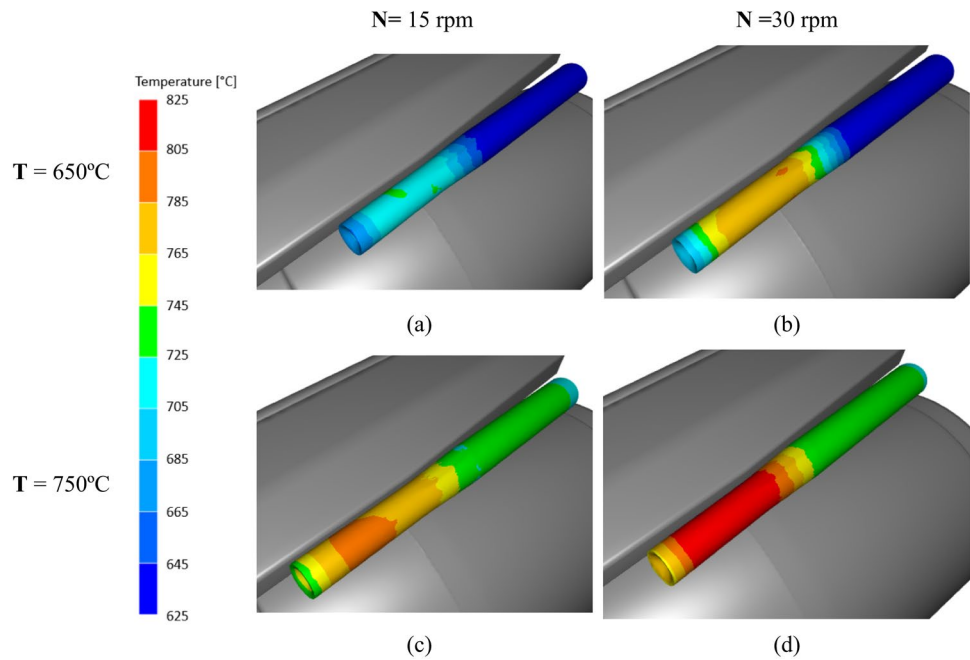
3.1 FE model results

The experimental area reduction of the rod in the skew rolling process (from initial diameter of 36 to final 30 mm) and final length of 432 mm have been compared to the simulation results. The average final diameter of the simulation is 30.59 mm, while the average final length is 440.5 mm. These results that were analyzed under warm conditions (without considering the posterior cooling to ambient temperature) confirm the validity of the model. In addition, recorded radial force, torque and velocity of the rod in the rolling direction are compared to simulation results in Fig. 5.

The results of velocity show a similar trend for all the simulated cases. The higher is the friction coefficient m , the closer are the results to the experiment. When the coefficient of friction reaches a certain value, increasing it does not substantially increase the velocity because the slip within the deformation zone is no longer reduced. This explains the small differences between the cases with $m=0.6$ and $m=0.65$. At low roll rotational velocities, the error compared to the experimental result is lower, while differences between the simulated cases are also minimum. Regarding those simulations with $m=0.65$, the highest deviation is shown for the temperature of 650 °C and rolls velocity of 30 rpm with a relative error (RE) of 10%. Simulation 9 shows the best accuracy with a RE of 4% (750 °C and 15 rpm).

Regarding torque, results put into evidence that the model is more accurate at the temperature of 750 °C. At this temperature, simulations with friction coefficient $m=0.55$ show the most accurate prediction (RE = 1% in Simulation 7), while at temperatures of 650 °C, simulations with $m=0.65$ are closer to the recorded values. Concerning rolls radial force, the difference between the simulated cases is negligible as the radial force is associated with compressing the material and reducing its cross section, which is not so closely linked to the contact conditions. The temperature has been found to be determinant, while the rotational velocity

Fig. 7 Temperature evolution during warm skew rolling of (a) case 1, (b) case 4, (c) case 9 and (d) case 12



shows a minimum impact. Simulations at 750 °C show good results, while at 650 °C radial forces are underestimated. It could be associated to a more accurate description of the material flow behavior at higher temperatures.

In order to understand the effect of friction on the material flow during the warm skew rolling process, the material surface twisting has been measured and compared to the simulations. This redundant deformation is linked to a different rotational velocity of the rod before and after the area reduction during the skew rolling. It is driven by the shear stress distribution in the contact area and leads mainly to differences in the sliding velocity in the contact regions during the manufacturing process. Surface twisting results are shown in Fig. 6.

As it can be observed, at 750 °C Simulations 9 and 12 ($m=0.65$) replicate the surface twisting of the material. Moreover, the higher is the friction coefficient, the higher is the surface twisting. It is explained by the lower sliding velocity at the contact (higher shear stress) that leads to a more severe material flow at the external layers of the rod

section. On the other hand, those simulations with lower friction and thus, higher sliding velocities, underestimate the surface twisting and, consequently, material flow.

At a temperature of 650 °C, Simulations 2 ($m=0.6$) and 4 ($m=0.55$) show the lowest deviation for rolling velocities of 15 and 30 rpm, respectively. The trend shown is similar to that previously explained for 750 °C. The higher the friction, the higher the surface twist. If we compare the twisting values, we can see that they are higher the higher the working temperature. This is related to the greater resistance to flow of the material at lower temperatures. With regard to rotational speed, it does not show direct influence on the surface torsion. The analysis of the rotation times (number of times the material contacts the rolls during its skew rolling) puts into evidence that it is not dependent on the roller’s rotational velocity and thus, the contact with rollers takes place at similar positions. As a result, the material flow in the surface is not modified by increasing or decreasing rollers rotational speed.

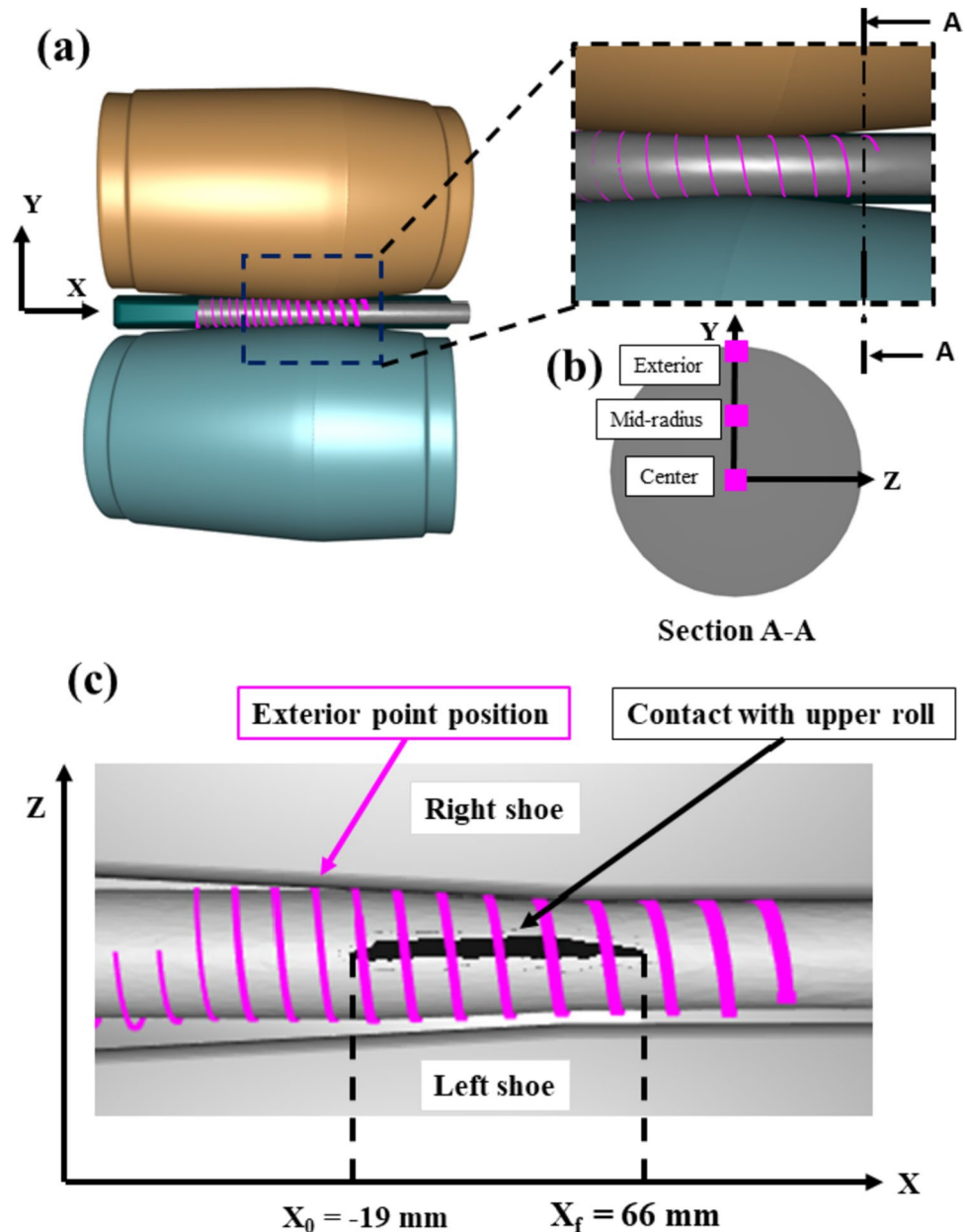
3.2 Process parameter analysis

In order to analyze the impact of process parameters on the mechanical properties and microstructure developed in the material, a series of simulations are analyzed. The selection of the simulation case that best reproduces each process condition (N, T) has been based on the twisting result, since the differences in terms of speed, radial force and torque are not substantial. This means that the friction of $m=0.55$ has been chosen for the 650 °C temperature, while $m=0.65$ for the 750 °C processes. The parameters to be studied are

Table 3 Temperature before and after the area reduction in the warm skew rolling mill

Case N°	Temperature after skew rolling (°C)	Initial temperature (°C)	ΔT (°C)
1	723.1	634.2	88.9
4	774.7	634.2	140.5
9	780.2	725.2	55
12	824.9	725.2	99.7

Fig. 8 Warm skew rolling mill (a) lateral view, (b) position of the three points in the billet section and (c) upper side view of the contact region with the upper roll and exterior contact point evolution



temperature, strain and strain rate. First, the temperature evolution in the surface of the rod is presented in Fig. 7.

The initial temperature is increased in the surface of the rod in all the analyzed cases. The temperature values before and after the area reduction in the skew rolling mill are shown in Table 3.

Results show that the initial temperature is the most determinant parameter defining the temperature rise in the surface of the rod during the skew rolling process. Cases 1 and 4 show a temperature increment of 88.9 and 140.5 °C, while cases 9 and 12 an increment of 65 and 99.7 °C, respectively. Despite the fact that the cases in which the initial temperature is higher present a higher friction coefficient value and, therefore, a higher heat generation in the interface, it can be

seen how the surface heating is lower. This is mainly due to two factors: on the one hand, a higher temperature promotes a higher thermal interaction with the tooling (accelerates heat loss). On the other hand, it confirms that the heating is mainly due to the adiabatic heating caused by the higher plastic deformation energy of the material at lower temperatures.

In order to analyze what happens inside the material, it was decided to record the evolution of the deformation conditions, namely temperature, strain rate and equivalent strain, at three points of the billet section, as illustrated in Fig. 8.

As it can be observed, the regions correspond to the surface, the mid-radius zone and the center, exactly at the

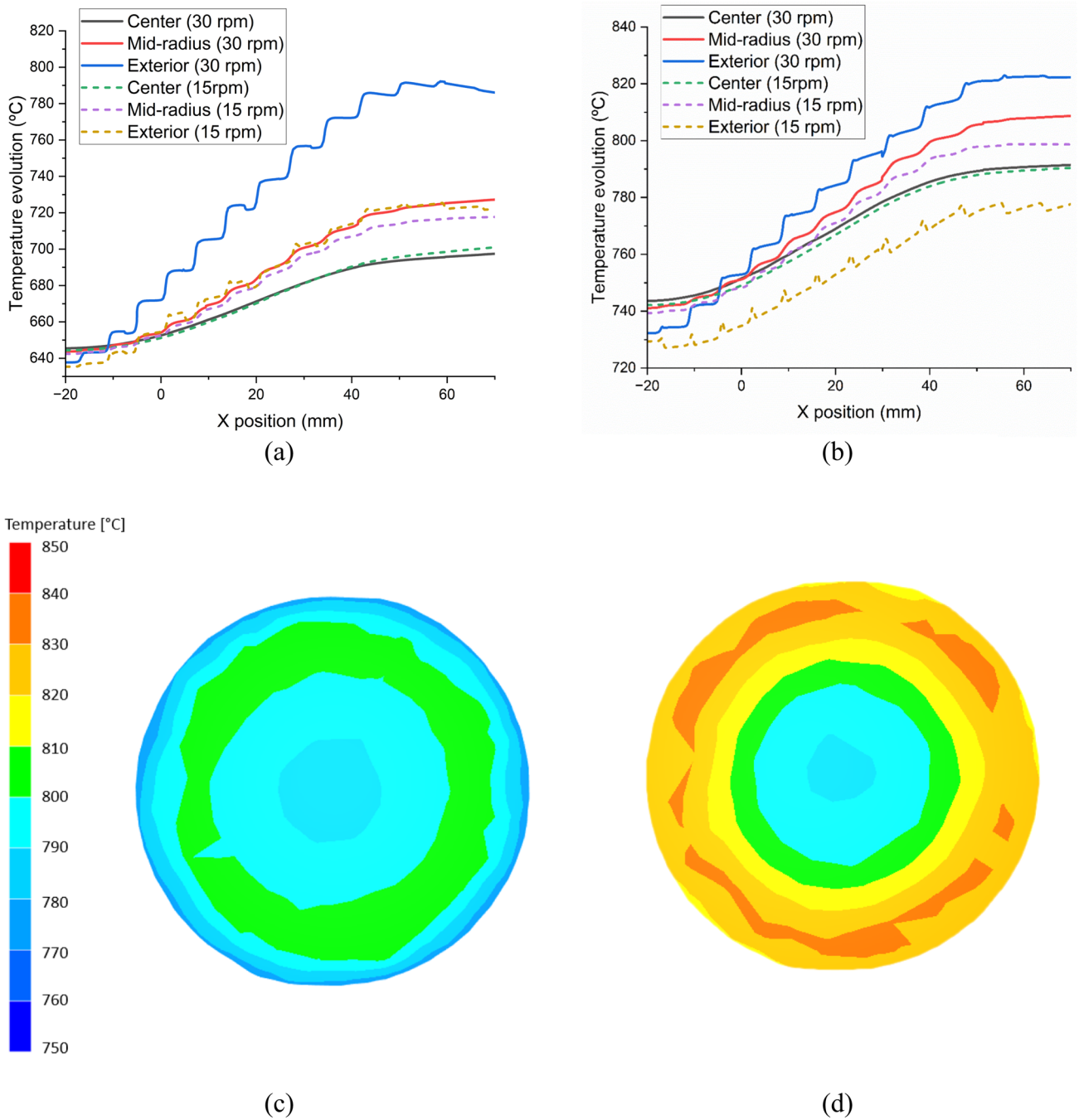


Fig. 9 Temperature evolution of the exterior, mid-radius and center with (a) starting temperature of 650 °C, (b) starting temperature of 750 °C. Furthermore, the temperature of the cross sections of (c) case 9 and (d) case 12 is provided

same locations where the microstructure of the material was initially measured. As previously introduced, the material contacts in barely the same axial position of rolls, independently on the temperature or rotational velocity considered. Therefore, instead of using the time frame to compare the different cases, the temperature evolution of the three points recorded during the WSR of the billet (shown in Fig. 8b) with respect to the X position is shown in Fig. 9, as well as

two sections of the temperature distribution in the section of cases 9 and 12.

According to the temperature evolution plots in Fig. 9a, it can be seen how, at lower temperatures, the heating effect due to a higher rotation speed is significant. This is especially noticeable in the temperature difference in the exterior zone, although it also occurs in the mid-radius zone, in the core of the billet the heating is independent of the rotation

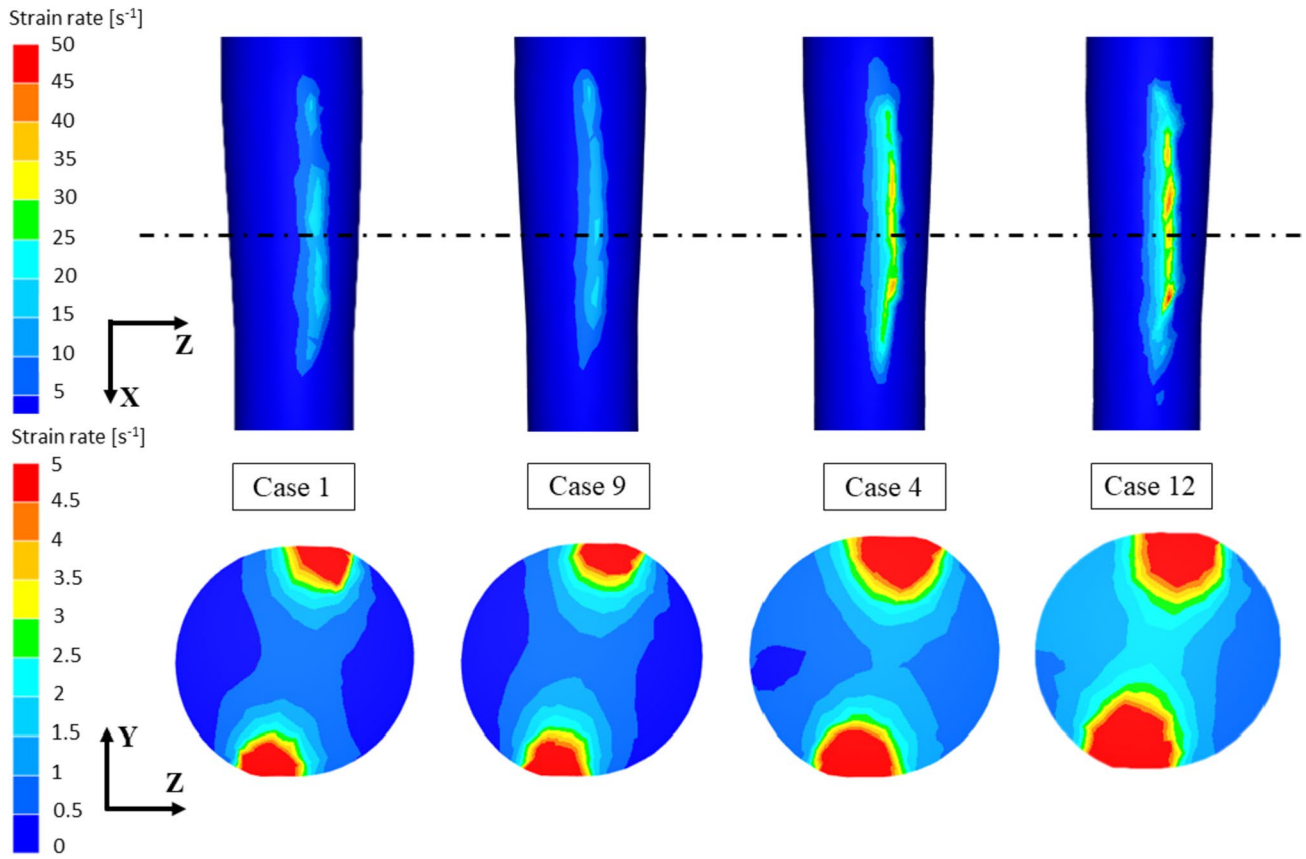


Fig. 10 Strain rate distribution in the surface and internal section of cases 1, 9, 4 and 12

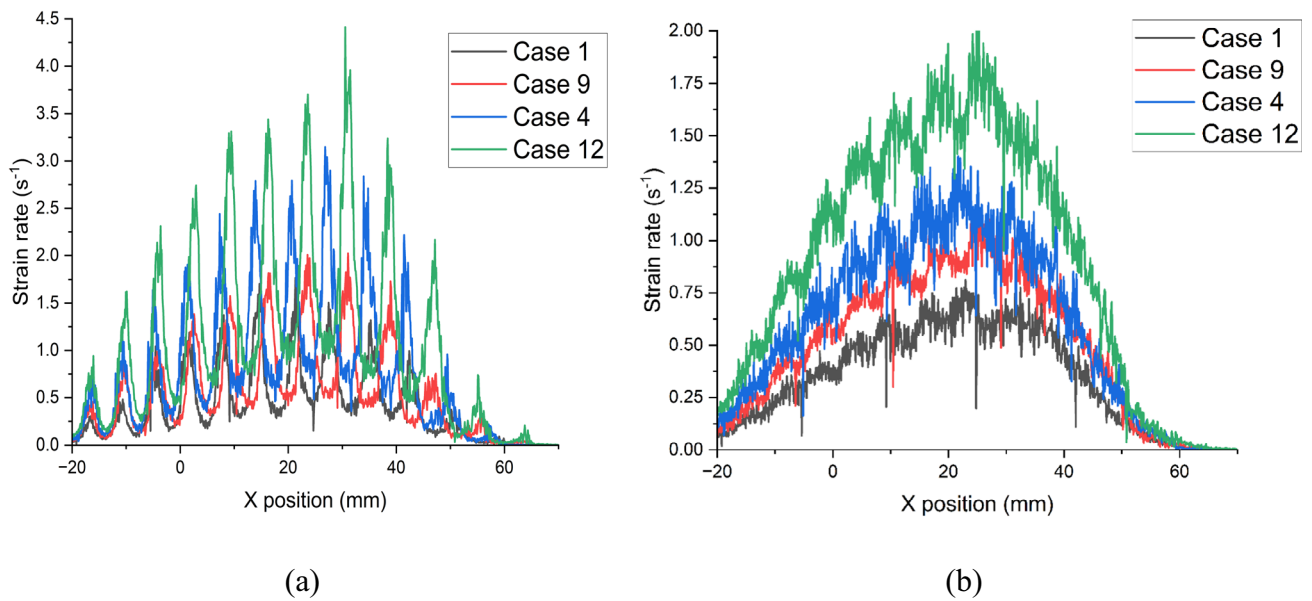


Fig. 11 Strain rate distribution in (a) mid-radius region and (b) center of the billet

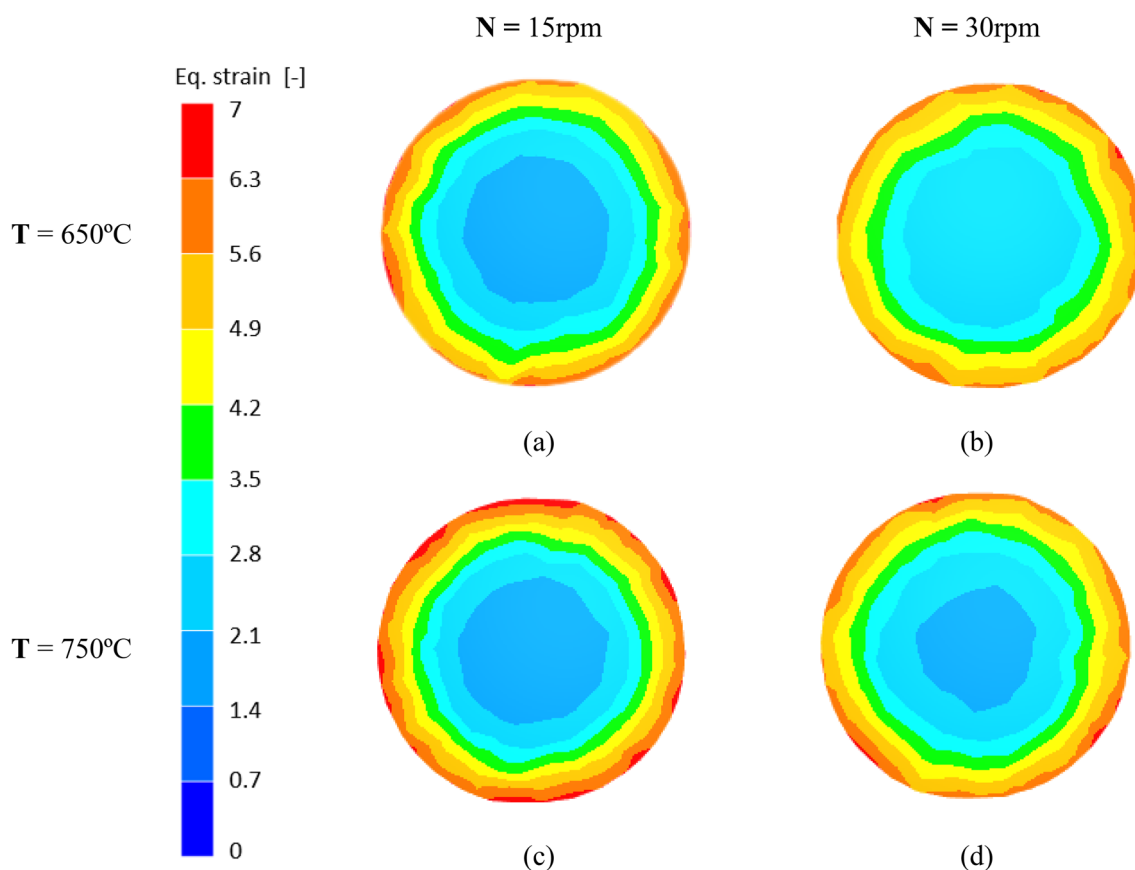


Fig. 12 Equivalent strain evolution during warm skew rolling of (a) case 1, (b) case 4, (c) case 9 and (d) case 12

speed. This is explained by the influence of the higher strain rate in the outermost layers of the billet section.

If results at 650 °C are compared with those at 750 °C, some differences can be appreciated. On the one hand, the outer zone shows a lower heating at 750 °C. This can be attributed to the high sensitivity of the material flow with

respect to temperature, leading to a lower plastic deformation work transformed into heat. Regarding the homogeneity of the temperature distribution, it is observed that in the cases at 15 rpm both present similar values, while if we compare cases 4 and 12 (both at 30 rpm), a more homogeneous distribution is observed the higher the initial temperature of the rod.

Figure 9c and d shows the difference in temperature distribution after WSR of cases 9 and 12, both starting at 750 °C, but with different strain rates. In case 9, a higher temperature loss can be observed in the core of the workpiece, while the distribution is more homogeneous. If the temperature distribution corresponding to case 12 is observed, the outer layers undergo a higher heating, despite the higher initial temperature loss, due to the effect of the strain rate. To examine the strain rate distribution during the process, Fig. 10 shows both the contact zone and the section at the point where the rollers have the lowest gap between them.

The first thing to note about the strain rate distribution during the process is that the strain rate values are much higher at the surface compared to the inner areas of the billet section. Therefore, it has been decided to use different scales in order to be able to analyze them independently.

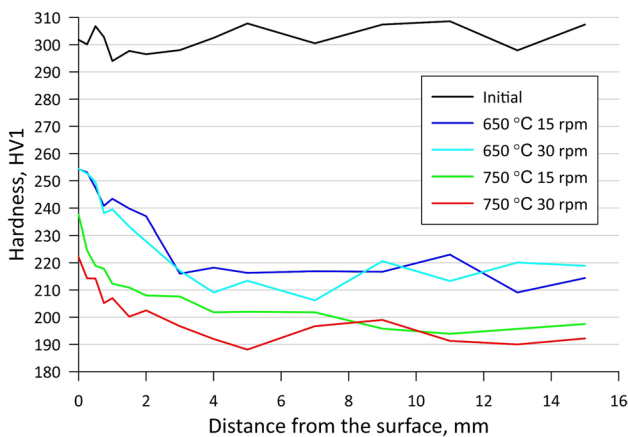
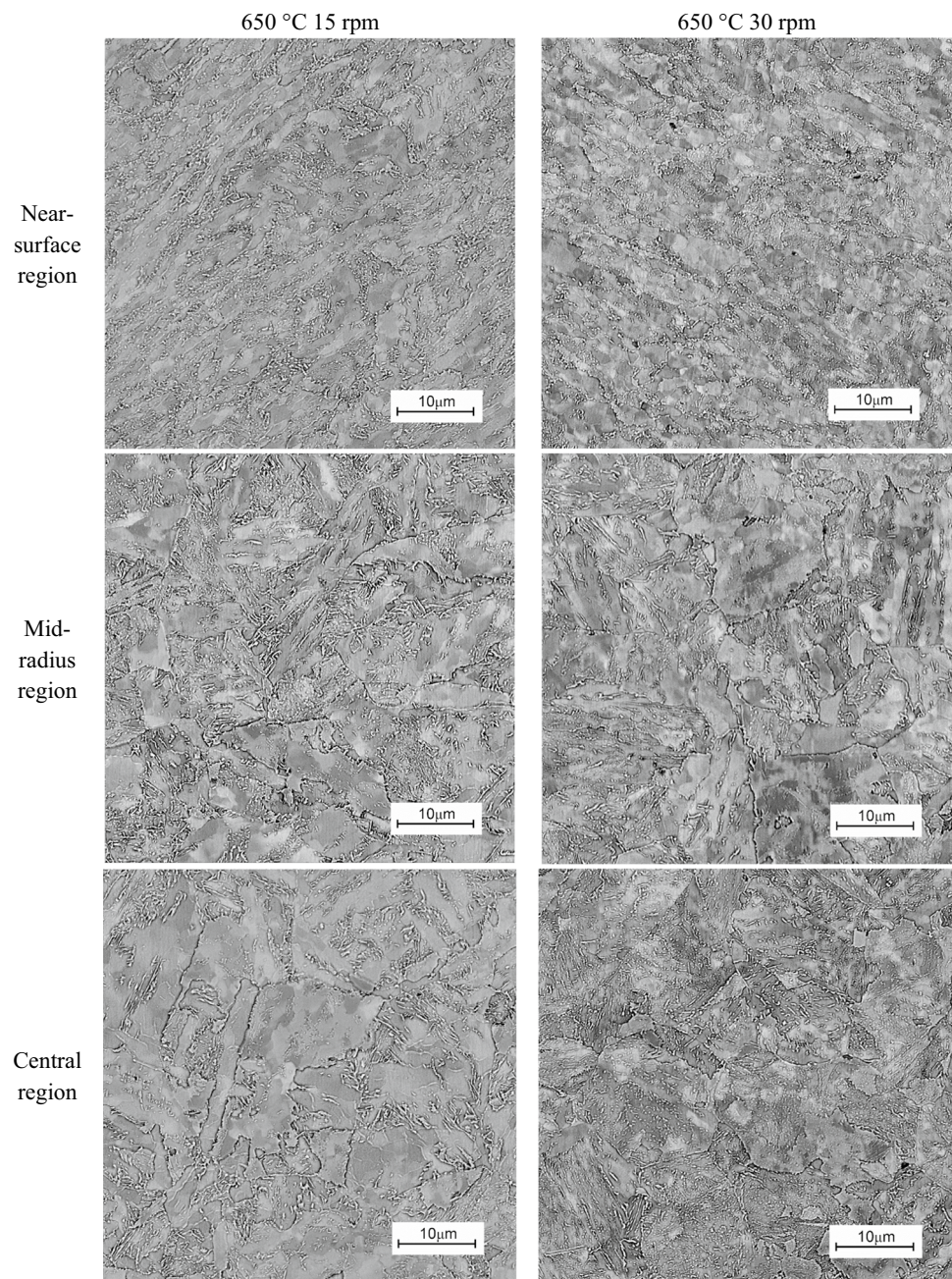


Fig. 13 Vickers hardness of the bars rolled at different conditions

Fig. 14 SEM micrograph of microstructure of bars rolled at 650 °C

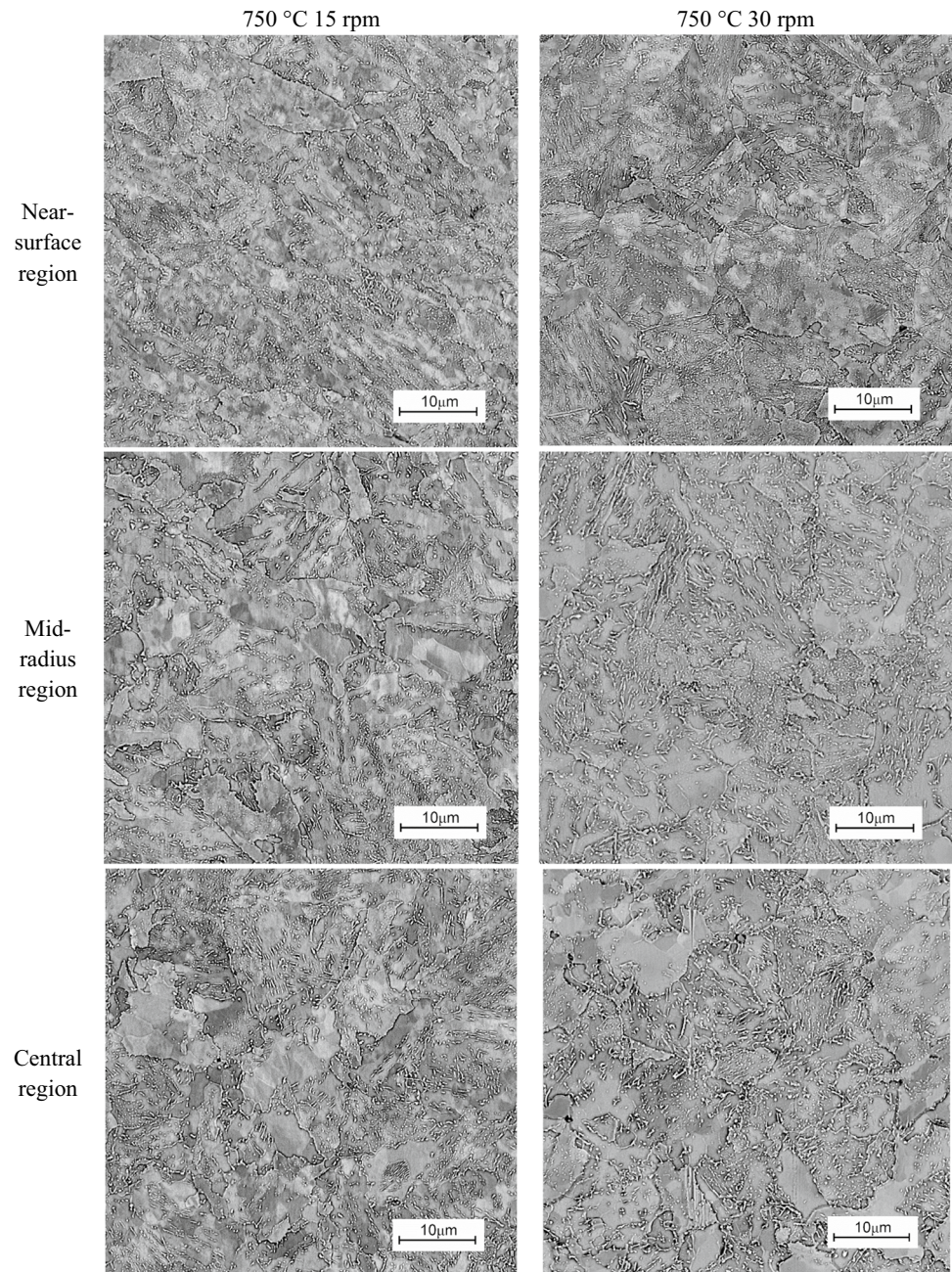


On the outer surface, in the area of contact with the roll, it is observed that between cases 1 and 9, as well as between cases 4 and 12, there are no appreciable differences. In cases 1 and 9, the strain rate is approximately 20 s^{-1} , while in cases 4 and 12, it is 40 s^{-1} . Therefore, the main parameter defining the strain rate is the rotational speed, while the initial temperature does not play such an important role. This differs if we focus on the inner area of the billet, as it can be seen that for similar values of rotational speed, there are

differences between the strain rate distribution in the section. In order to evaluate this in greater detail, Fig. 11 shows a comparison of the values in the area of the core and the mid-radius.

From the mid-radius results shown in Fig. 11a, it can be observed how by increasing the rotation speed from 15 to 30 rpm, the strain rate doubles its value each time the section comes into contact with the roller (strain rate peaks in the graph). Regarding the initial temperature, it can be seen

Fig. 15 SEM micrograph of microstructure of bars rolled at 750 °C



that it has an influence on the strain rate, although it is lower compared to the rotation speed of the roll. In the cases corresponding to 750 °C, the strain rate values are higher for equal rotation speed, slightly displacing the contact points of the material with the rolls.

Figure 11b puts into evidence that the strain rate distribution shows less oscillations with a lower amplitude in the central area of the rod. Similar to the mid-radius region, higher strain rate values are observed the higher the temperature and rotational speed of the rollers. Finally, to investigate

the effect of strain rate fluctuations on the resulting strain distribution in the material, Fig. 12 is shown.

From results of Fig. 12, it can be concluded that equivalent strain in the outer radius of the rod shows a similar distribution and value in all the analyzed cases. This can be explained by the balance existing among the material strain rate and contact time, given that in all the examined cases the rotation times and position where material contacts the roll are similar. However, some differences can be appreciated in the internal region of the rod. Since the higher the rotational speed, the more similar the strain rate values

Table 4 DoS of the resulting WSR microstructure

Temperature (°C)	Rotational velocity (rpm)	Zone	DoS
–	–	Initial microstructure	0.144
650	15	Near-surface	0.544
		Mid-region	0.332
		Central	0.176
650	30	Near-surface	0.493
		Mid-region	0.193
		Central	0.169
750	15	Near-surface	0.792
		Mid-region	0.608
		Central	0.356
750	30	Near-surface	0.865
		Mid-region	0.589
		Central	0.514

are between the outer and inner regions and thus the more homogeneous the strain distribution becomes. Nevertheless, the initial temperature does not affect it in the same way, as greater homogeneity is observed at lower temperatures, with the effect being less noticeable.

3.3 Mechanical properties and microstructure

The mechanical properties of the rolled bars were characterized by means of hardness measurements performed on the cross section of the bars: initial and rolled bars under different conditions. Hardness tests were carried out using the Vickers method at a load of 1000 g. It was deliberately not tested using lower loads so that the tests were macroscopic and the results averaged out the structural composition of the material. Testing was carried out along a path from the surface toward the core of the bar with varying spacing. A smaller distance was used at the surface due to the nature of the strain. The results of the hardness measurements are summarized as a graph in Fig. 13.

The analysis of the hardness measurement results shows that the material in the initial state has the highest hardness among the samples tested. The hardness ranges from 294 to 308.6 HV1 with an average value of 302 HV1. Despite slight fluctuations in the hardness level occurring close to the surface, no significant changes were observed over the cross-section of the sample.

The hardness obtained for the rolled samples is significantly lower compared to the initial sample. In all cases, a decrease in hardness was observed from the surface toward the core to a depth of 3–4 mm, where the results stabilize. Samples rolled at 650 °C, compared to those rolled at 750 °C, obtained higher hardness results at all measurement

points. Samples that were rolled at a lower roll rotational velocity (15 rpm) also have a higher hardness.

The decrease in hardness in the sample cores is thus dependent on the process temperature and the rotational velocity of the rollers. The higher these parameters are, the greater the decrease in hardness relative to the initial sample is observed. Although lower than the initial value, there is a higher hardness at the near-surface region compared to the mid-radius and core regions, which corresponds to the high strain zone according to the simulation for all the analyzed cases (see Fig. 12). In general, for all the cases analyzed, a marked decrease in hardness was observed and, in order to investigate its relationship with the resulting microstructure, SEM micrographs were done in the external, mid-radius and core regions of the rod. Figures 14 and 15 present, respectively, the microstructure of bars rolled at 650 and 750 °C.

Microstructural modifications were observed as a result of rolling, the extent of which depends on the process conditions. Rolling at 650 °C resulted in a significant breakdown of the cement platelets in the near-surface region for both 15 and 30 rpm rolling velocities. This can be related to the strain rate peaks occurring in the area outside the roller contact under all conditions studied according to the simulation (see Fig. 10). In both cases, the banded structure obtained is visible. With a roller velocity of 30 rpm, significant fragmentation of the cementite platelets and deformation (flattening) of the ferritic areas extends to the mid-zone. In Fig. 11a, simulation showed high strain rate values concentrated in the middle zone only in the case of 30 rpm and 650 °C, which could explain the flattening phenomenon. In the central zone, only minor structural changes are visible, relative to the original material. This aligns with the low strain rate values located in the core, with the lowest values occurring at the lowest temperature and rotational speed of the roll (see Fig. 11b). For specimens rolled at 750 °C, significant degradation of the pearlitic platelet structure and mixing of the fine particles with the ferritic matrix is observed in the near-surface zone. Again, banding can be observed. In the intermediate zone, significant structural changes were observed for both velocities considered; however, the extent of mixing of the components is noticeably greater for the 30 rpm roll velocity. In the central zones, the effect of the rolling process on the structural morphology was also observed. The pearlite plates are degraded to a degree similar to that observed in the intermediate zones for each strain rate. From the simulation results of strain rate, it was observed that the higher was the temperature, the higher were the values of strain rate in the mid-radius and core (see Fig. 10). Therefore, this could favor the mixing of the components.

In order to analyze the microstructure in more detail, additional micrographs were taken. The degree of

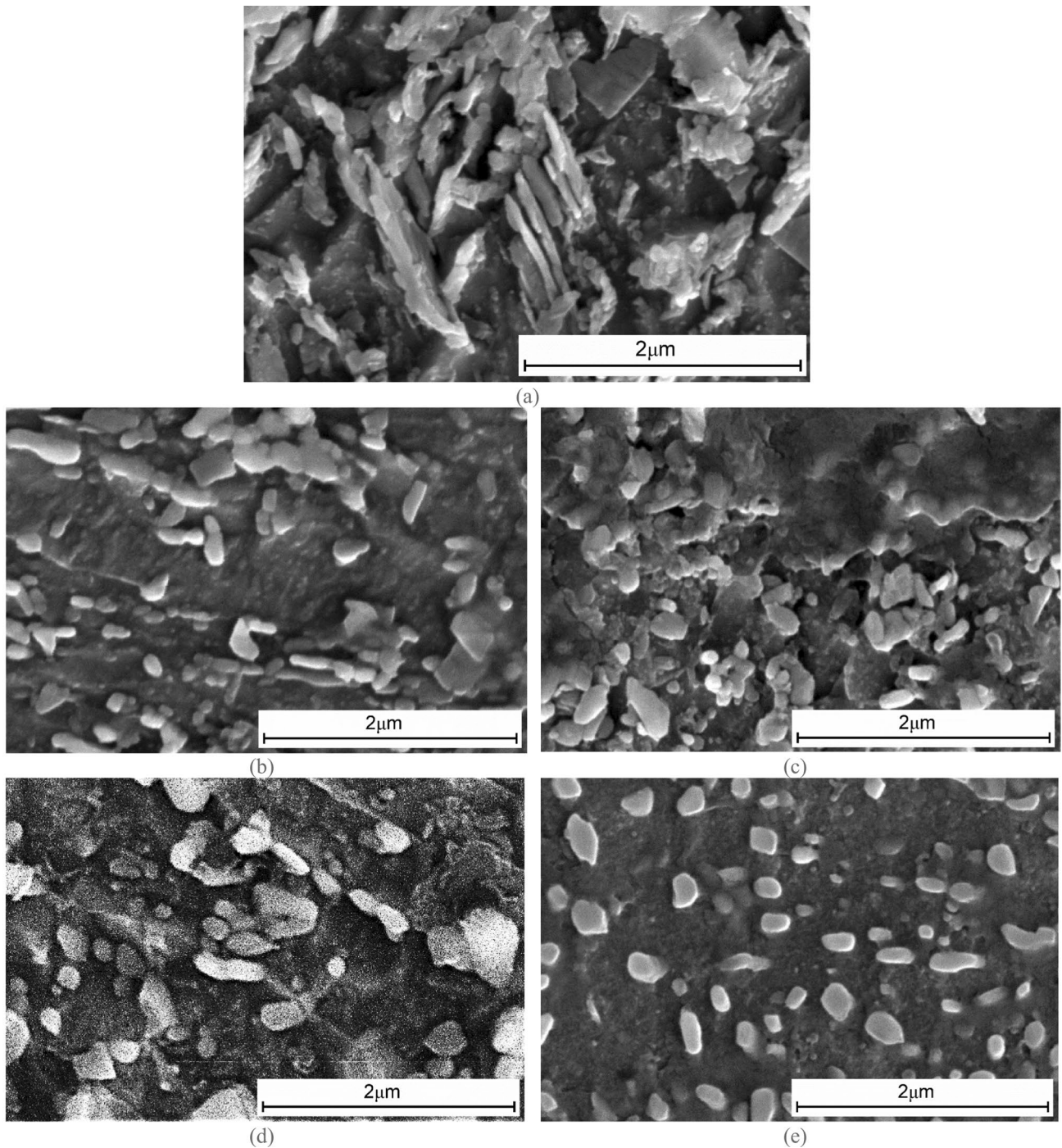


Fig. 16 Cementite precipitates, in the near-surface zone of samples: (a) initial, (b) 650 °C and 15 rpm, (c) 650 °C and 30 rpm, (d) 750 °C and 15 rpm, (e) 750 °C and 30 rpm. Etched with picral 5%, then with Nital 4%

spheroidization (DoS) was determined based on the ratio of the average width of cementite particles to their length and was determined in the areas near the surface, in the middle of the radius and in the central zone. Measurements were made based on the aforementioned SEM micrographs. Approximately 100 measurements were considered for three

reference areas of $10 \times 10 \mu\text{m}$ in each of the analyzed zones. The results of spheroidization from 0 (lamellar) to 1 (spheroidal) are listed in Table 4.

From results of Table 4, it can be stated that both an increase in temperature, and roll velocity, increase the extent

of structural modification in the steel under test. Nevertheless, an increase in temperature has a greater effect on this extent. As a result of the breakdown of the cementite plates, the modified microstructure is not similar to that of the initial pearlite. The warm-rolled modified microstructure shows great similarity to the spheroidal microstructure. In order to assess the morphology of the resulting precipitates, SEM captions with higher magnification are shown in Fig. 16.

Detailed observations of pearlitic precipitates presented in Fig. 16 reveal significant morphological differences between the rolled samples and the initial sample. Thanks to the use of two-stage etching, conglomerates of pearlite plates with angular shapes were revealed for the initial sample (Fig. 16a). Precipitates of this type are related to the classic pearlitic transformation during steel normalization. The morphology of cementite precipitates after rolling tests (Fig. 16b–e) differs significantly due to their greater fragmentation and progressive spheroidization of shape with increasing temperature and roll rotational speed during WSR. The mechanism of fragmentation and spheroidization of cementite may occur with the participation of divorced eutectoid transformation and may be supported by deformation-induced transformation. Both in the case of samples rolled from an initial temperature of 650 and 750 °C, at the end of the process, the outer layers of the bar are above the temperature A1.

A large share of fragmented but not dissolved cementite precipitates promotes divorced eutectoid transformation, which upon cooling results in approximately spherical precipitates with rounded shapes. A greater roll rotational speed during the process (Fig. 16c, e) increases strain rate, which favors mixing of the material and thus the share of small precipitates arranged in rows (one after the other) is sensibly smaller compared to these samples rolled longer time (Fig. 16b, d). The highest DoS and dispersion of precipitates were obtained for the sample rolled at 750 °C and 30 rpm.

In order to assess crystallographic orientation and grain boundaries, an analysis of the near-surface areas, at a distance of approximately 4 mm from the surface of the bars, was performed using the EBSD. The results are illustrated in Fig. 17.

The grain size homogeneity of the initial sample (Fig. 1) is clearly the largest for the area analyzed. Rolled samples 17a–d are characterized by larger grain size differences. The average grain size determined by the EBSD method is at a similar level for the initial sample and the samples rolled at 30 rpm. In the case of the samples rolled at 15 rpm, smaller grain sizes of approximately 40% were observed compared to the other samples. This is most likely due to the highest temperature reached at the end of the higher speed rolling process.

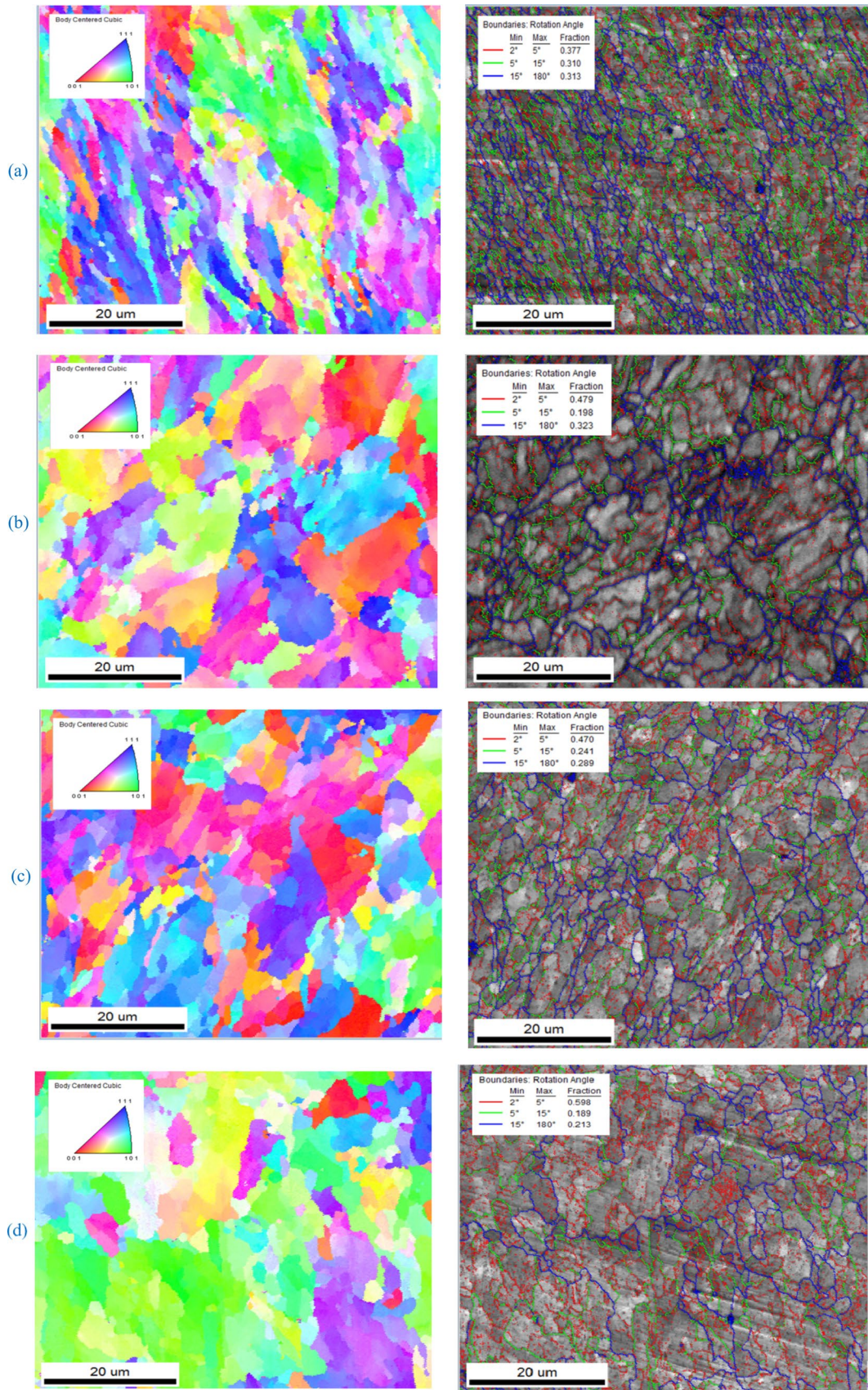
Considering the distribution of the angular disorientation of the grain boundaries, it can be observed that for all samples there is a higher proportion of low-angle boundaries. When comparing rolled samples that have cementite in spheroidal form, the highest percentage of high angular boundaries is found for samples rolled at a temperature of 650 °C and is approximately 32%. As the rolling temperature increases, the proportion of high-angle boundaries decreases and reaches, for the case of 750 °C and 30 rpm, the minimum value of 21.3%. Highly angular boundaries are characterized by increased dislocation density, which thus translates into increased mechanical properties [25]. The results found are in line with the results of hardness measurements, where a decrease in hardness was obtained with an increase in rolling temperature.

An increase in temperature achieves a microstructure morphology close to the original in terms of grain size and shape while maximizing the softening effect. Rolling from lower temperatures favors grain fragmentation and the achievement of incomplete spheroidization, which, in combination with the highest proportion of high-angle boundaries, contributes to a higher hardness of the bars with respect to those rolled at higher temperatures. Despite the convergence of the morphological parameters of the grain microstructure for the initial sample and that rolled at 750 °C and 30 rpm, the decisive factor that maximizes the softening effect is the change in the form of the cementite precipitates to the spheroidal form with the greatest degree of dispersion. WSR enables cementite spheroidization by exploiting the phenomenon of divorced eutectoid transformation. Compared to traditional softening annealing methods, the spheroidization method of WSR can be much more efficient in terms of time and energy savings.

4 Conclusions

In this article, the WSR process is modeled by the finite element method. The effects of warm forming parameters, namely initial temperature and roll rotational velocity, on the material strain rate, thermal properties, microstructure and hardness were analyzed. Experimental data validated the simulation results. The initial microstructure consisting of a ferritic–pearlitic structure with regular grains was transformed by spheroidization of the cementite exploiting the phenomenon of divorced eutectoid transformation and the breakdown of the cementite plates. The conclusions are presented below:

- The contact conditions in the warm skew rolling process have been investigated. The material flow is highly dependent on the existing friction with the rolls and



◀**Fig. 17** Results of the EBSD analysis: misorientation profile map—left, grain boundary misorientation right: (a) 650 °C and 15 rpm, (b) 650 °C and 30 rpm, (c) 750 °C and 15 rpm, (d) 750 °C and 30 rpm

temperature plays a fundamental role. It has been found that the friction is higher at 750 °C ($m = 0.65$) compared to its value at 650 °C ($m = 0.55$), leading to a higher material twisting at higher temperature.

- The initial temperature plays a fundamental role in heating and temperature distribution. In the cases analyzed with an initial temperature of 650 °C, the surface heating is 88.9 °C (15 rpm) and 140.9 °C (30 rpm), while those with an initial temperature of 750 °C have 55 °C (15 rpm) and 99.7 °C (30 rpm), respectively. Moreover, the homogeneity is higher when the initial temperature is 750 °C. This is due to the fact that the core heats up in a similar way regardless of the rotation speed and temperature with an average value of 47 °C. Regarding the rotation speed, the 30 rpm cases favor a higher heating due to the shorter operation time, as well as a higher strain rate, which is mainly concentrated in the outermost layers of the rod and results in adiabatic heating.
- The hardness levels attained after WRS consistently fall below the average initial hardness of 302 HV1 across all scenarios. Notably, greater softening is evident in the mid-radius and core regions as compared to the near-surface zone. Specifically, a more pronounced reduction in hardness occurs at a temperature of 750 °C, with higher rotational speeds of the roller contributing to increased softening effects. The case corresponding to 750 °C and 30 rpm demonstrates the most substantial reduction in hardness. In the near-surface region (external layer within 2 mm), the average hardness diminishes to 209.4 HV1, representing a 30.7% decrease, while in the mid-radius and central regions, the average hardness is 194.1 HV1, leading to a 35.7% reduction.
- Increasing the temperature yields a microstructure morphology that closely approximates the original, characterized by comparable grain size and shape, thereby maximizing the associated softening effect. Conversely, rolling at lower temperatures fosters grain fragmentation and the attainment of incomplete spheroidization, accompanied by a higher prevalence of high-angle boundaries, thereby contributing to elevated hardness in the resulting bars in comparison to those subjected to higher temperature rolling.
- The DoS is increased with deformation, but mainly with temperature. The maximum values of 86.5 and 79.2% occur at an initial temperature of 750 °C in the near-surface zone, which is heated the most. The DoS of core and mid-radius are comparable to the near-surface zone for cases starting at 650 °C, as they achieve similar temperatures.

- Despite the convergence of morphological parameters in the grain microstructure between the initial sample and the specimen rolled at 750 °C and 30 rpm, the main factor driving the maximization of the softening effect lies in the transformation of cementite precipitates into a spheroidal form characterized by the greatest degree of dispersion.

Acknowledgements This study received financial support from the Department of Education of the Basque Government for the Research Group program IT1507-22. The research was financed from the funds of the Scientific Discipline Council for Mechanical Engineering: M/KOPM/FD-20/IM-5/013/2022.

Author's contribution AM-M and TB contributed to conceptualization; AM-M, TB, and HAD provided methodology; AM-M, TB, and HAD performed formal analysis and investigation; AM-M and TB performed writing—original draft preparation; HAD, EG, KM, JT, and ZP performed writing—review and editing; TB, EG, and ZP contributed to resources; EG, KM, JT, and ZP performed supervision.

Funding Open Access funding provided thanks to the CRUE-CSIC agreement with Springer Nature.

Data availability The data that support the findings of this study are available from the corresponding author, AM-M, upon reasonable request.

Declarations

Conflict of interest The authors declare no conflict of interest.

Open Access This article is licensed under a Creative Commons Attribution 4.0 International License, which permits use, sharing, adaptation, distribution and reproduction in any medium or format, as long as you give appropriate credit to the original author(s) and the source, provide a link to the Creative Commons licence, and indicate if changes were made. The images or other third party material in this article are included in the article's Creative Commons licence, unless indicated otherwise in a credit line to the material. If material is not included in the article's Creative Commons licence and your intended use is not permitted by statutory regulation or exceeds the permitted use, you will need to obtain permission directly from the copyright holder. To view a copy of this licence, visit <http://creativecommons.org/licenses/by/4.0/>.

References

1. Pater Z, Tomczak J, Bulzak T, Wójcik Ł, Skripalenko MM. Prediction of ductile fracture in skew rolling processes. *Int J Mach Tools Manuf.* 2021;163: 103706. <https://doi.org/10.1016/j.ijmactools.2021.103706>.
2. Zhang H, Wang B, Lin L, Feng P, Zhou J, Shen J. Numerical analysis and experimental trial of axial feed skew rolling for forming bars. *Arch Civ Mech Eng.* 2021;22:17. <https://doi.org/10.1007/s43452-021-00334-z>.
3. Yamane K, Shimoda K, Kuroda K, Kajikawa S, Kuboki T. A new ductile fracture criterion for skew rolling and its application to evaluate the effect of number of rolls. *J Mater Process Technol.* 2021;291: 116989. <https://doi.org/10.1016/j.jmatprotec.2020.116989>.

4. Kache H, Stonis M, Behrens B-A. Development of a warm cross wedge rolling process using FEA and downsized experimental trials. *Prod Eng.* 2012;6:339–48. <https://doi.org/10.1007/s11740-012-0379-5>.
5. Behrens B-A, Suchmann P, Schott A. Warm forging: new forming sequence for the manufacturing of long flat pieces. *Prod Eng.* 2008;2:261–8. <https://doi.org/10.1007/s11740-008-0114-4>.
6. Huang X, Wang B, Zhou J, Ji H, Mu Y, Li J. Comparative study of warm and hot cross-wedge rolling: numerical simulation and experimental trial. *Int J Adv Manuf Technol.* 2017;92:3541–51. <https://doi.org/10.1007/s00170-017-0399-6>.
7. Maropoulos S, Ridley N. Inclusions and fracture characteristics of HSLA steel forgings. *Mater Sci Eng A.* 2004;384:64–9. <https://doi.org/10.1016/j.msea.2004.05.023>.
8. Costa LL, Brito AMG, Rosiak A, Schaeffer L. Microstructure evolution of 42CrMo4 during hot forging process of hollow shafts for wind turbines. *Int J Adv Manuf Technol.* 2020;106:511–7. <https://doi.org/10.1007/s00170-019-04642-w>.
9. Bayrak M, Ozturk F, Demirezen M, Evis Z. Analysis of tempering treatment on material properties of DIN 41Cr4 and DIN 42CrMo4 steels. *J Mater Eng Perform.* 2007;16:597–600. <https://doi.org/10.1007/s11665-007-9043-1>.
10. Diefenbach J, Brunotte K, Behrens B-A. Microstructure and Mechanical Properties of Thermomechanically Forged Tempering Steel 42CrMo4. In: Behrens B-A, Brosius A, Hintze W, Ihlenfeldt S, Wulfsberg JP, editors. *Prod. Lead. Edge Technol.*, Berlin, Heidelberg: Springer Berlin Heidelberg; 2021, p. 142–50.
11. Szala M, Winiarski G, Wójcik Ł, Bulzak T. Effect of annealing time and temperature parameters on the microstructure, hardness, and strain-hardening coefficients of 42CrMo4 steel. *Materials.* 2020;13:2022. <https://doi.org/10.3390/ma13092022>.
12. Hu J, Du L-X, Xie H, Yu P, Misra RDK. A nanograined/ultrafine-grained low-carbon microalloyed steel processed by warm rolling. *Mater Sci Eng A.* 2014;605:186–91. <https://doi.org/10.1016/j.msea.2014.03.064>.
13. Xiong Y, Sun S, Li Y, Zhao J, Lv Z, Zhao D, et al. Effect of warm cross-wedge rolling on microstructure and mechanical property of high carbon steel rods. *Mater Sci Eng A.* 2006;431:152–7. <https://doi.org/10.1016/j.msea.2006.05.148>.
14. Shu X, Shi J, Chen J, Yang H. Effects of process parameters on surface quality of shaft parts formed by warm cross-wedge rolling. *Int J Adv Manuf Technol.* 2021;113:2819–31. <https://doi.org/10.1007/s00170-021-06784-2>.
15. Sun SH, Xiong Y, Zhao J, Lv ZQ, Li Y, Zhao DL, et al. Microstructure characteristics in high carbon steel rod after warm cross-wedge rolling. *Scr Mater.* 2005;53:137–40. <https://doi.org/10.1016/j.scriptamat.2005.01.011>.
16. Lee Y, Yoon E, Nho T, Moon Y. Microstructure control of ferrous driven part fabricated by warm precision forging. *Procedia Manuf.* 2018;15:404–10. <https://doi.org/10.1016/j.promfg.2018.07.236>.
17. Cui M-C, Zhao S-D, Zhang D-W, Chen C, Li Y-Y. Finite element analysis on axial-pushed incremental warm rolling process of spline shaft with 42CrMo steel and relevant improvement. *Int J Adv Manuf Technol.* 2017;90:2477–90. <https://doi.org/10.1007/s00170-016-9566-4>.
18. Serajzadeh S. Modelling the warm rolling of a low carbon steel. *Mater Sci Eng A.* 2004;371:318–23. <https://doi.org/10.1016/j.msea.2003.12.007>.
19. Koohbor B, Ohadi D, Serajzadeh S, Akhgar JM. Effect of rolling speed on the occurrence of strain aging during and after warm rolling of a low-carbon steel. *J Mater Sci.* 2010;45:3405–12. <https://doi.org/10.1007/s10853-010-4365-z>.
20. Serajzadeh S, Mohammadzadeh M. Effects of deformation parameters on the final microstructure and mechanical properties in warm rolling of a low-carbon steel. *Int J Adv Manuf Technol.* 2007;34:262–9. <https://doi.org/10.1007/s00170-006-0594-3>.
21. Huo Y, He T, Wang B, Zheng Z, Yang W, Hu Y, et al. Forming analysis of steel ball bearings made with warm skew rolling. *Mater Technol.* 2020;54:417–22. <https://doi.org/10.17222/mit.2019.201>.
22. Huo Y, He T, Wang B, Zheng Z, Xue Y. Numerical prediction and experimental validation of the microstructure of bearing steel ball formation in warm skew rolling. *Metall Mater Trans A.* 2020;51:1254–63. <https://doi.org/10.1007/s11661-019-05589-z>.
23. Murillo-Marrodán A, Garcia E, Barco J, Cortés F. Analysis of wall thickness eccentricity in the rotary tube piercing process using a strain correlated FE model. *Metals.* 2020;10:1045. <https://doi.org/10.3390/met10081045>.
24. Murillo-Marrodan A, Garcia E, Cortes F. A Study of friction model performance in a skew rolling process numerical simulation. *Int J Simul Model.* 2018;17:569–82. [https://doi.org/10.2507/IJSIMM17\(4\)441](https://doi.org/10.2507/IJSIMM17(4)441).
25. Najafi S, Eivani AR, Samaee M, Jafarian HR, Zhou J. A comprehensive investigation of the strengthening effects of dislocations, texture and low and high angle grain boundaries in ultrafine grained AA6063 aluminum alloy. *Mater Charact.* 2018;136:60–8. <https://doi.org/10.1016/j.matchar.2017.12.004>.

Publisher's Note Springer Nature remains neutral with regard to jurisdictional claims in published maps and institutional affiliations.